Korean J. Chem. Eng., 39(6), 1450-1459 (2022)
DOI: 10.1007/s11814-022-1068-5

pISSN: 0256-1115
eISSN: 1975-7220

Biodiesel production from waste cooking oil employing natural bentonite supported heterogeneous catalyst: Waste to biodiesel

Abdul Naeem*,†, Shah Zaman*,†, Muhammad Farooq*,†, Ihtisham Wali Khan*, Zahid Ali Ghazi*, Tooba Saeed*, and Muhammad Hamayun**

*National Centre of Excellence in Physical Chemistry, University of Peshawar, Peshawar Pakistan
**Department of Chemistry, University of Gujrat, Pakistan
(*Received 8 September 2021 • Revised 3 January 2022 • Accepted 13 January 2022*)

Abstract−This work describes the practicability of utilizing bentonite clay as a cheap and raw support for heterogeneous catalyst development. In the current research, ammonium persulfate (APS) impregnated bentonite heterogeneous catalyst was designed for the conversion of waste cooking oil to biodiesel. The fabricated catalyst was analyzed by various instrumental techniques (FTIR, TGA, BET, SEM, XRD, and EDX) to study its various physiochemical properties. It was identified that the clay supported heterogeneous catalyst executed an excellent activity for waste cooking oil conversion as providing maximum biodiesel yield of 93% at optimal reaction conditions (reaction temperature 75 °C, oil/methanol molar ratio, 1 : 10; catalyst amount, 2.5 wt%; stirring rate, 600-rpm in 3.5 hr reaction time). Gas chromatography mass spectroscopy (GCMS) analysis confirms the successful conversion to biodiesel. Similarly, the various physiochemical characteristics of the synthesized biodiesel meet the international standard of American (ASTM6751) and European Union (EU-14214). Moreover, the designed acid catalyst showed catalytic activity for up to eight consecutive runs demonstrate its good reusability.

Keywords: Bentonite, Ammonium Persulphate (APS), Transesterification, Biodiesel, Reusability

INTRODUCTION

Energy resources make a significant contribution in the development of human society. Presently, fossil fuels are the mainstream of energy all over the world. Fossil fuel provides about 85% of the world's commercial energy [1]. However, in the last three decades, prominent attention has emerged to overcome the future energy crises for transportation and industrially sufficient societies. Therefore, it is essential to search for the renewable energy sources to minimize the dependency on fossil fuel. Among different renewable energy sources, biodiesel has attracted great attention worldwide due to its renewability, environmentally friendly behavior, sulfur free, safe, and sustainability [2]. Moreover, it has high ignition value due to superior flash point (>130 °C) and is considered as an excellent alternative source of energy [3,4]. Chemically, biodiesel is a mixture of long chain fatty acid mono alkyl esters derived from vegetable oils or animal fats by the process of trans-esterification reaction [5]. Recent studies have indicated that the cost of biodiesel is a major barrier to its industrialization. It has been reported that 70-95% biodiesel cost is concerned with the cost of feedstock [6,7]. Currently, about 95% of biodiesel is mainly produced from edible oils [8,9]. The boundless use of edible oils may cause starvation in the poor and developing countries. As a result, several attempts have been made to select a suitable feedstock for sustainable biodiesel production in the future. Apropos to the above, waste-cooking oil (WCO: waste product of many hotels, restaurants and homes) may be an encouraging indigenous waste material for biodiesel production in the near future.

Similarly, different homogeneous and heterogeneous catalysts have been employed to carry out the conventional trans-esterification process. Although homogeneous catalysts (acid/base) give higher biodiesel yield under the temperate reaction conditions, these catalysts cause serious problems such as soap formation, tremendous amounts of waste water production, reactor corrosion and reduce the overall cost of biodiesel [10-12]. Therefore, heterogeneous catalysts are most acceptable in biodiesel technology to overcome the problems associated with homogeneous catalysts. Heterogeneous catalysts offer several advantages, such as environmentally friendly behavior, recyclability, prevent reactor corrosion, easy separation, and providing ester and glycerol of high purity [13,14]. Moreover, heterogeneous acid catalysts are ideal for the conversion of non-edible low cost feedstock of high free fatty acid contents as they carry simultaneous esterification and transesterification reaction, and thereby improves the overall process efficiency [15,16].

Various researchers have investigated a variety of heterogeneous catalysts for the catalytic trans-esterification of edible, non-edible oil vegetable oil for biodiesel production. Goncalves et al. designed $MoO_3/SrFe_2O_4$ heterogeneous acid catalyst for biodiesel production utilizing WCO. The maximum biodiesel yield achieved was 95.4% [17]. Al-Saadi et al. synthesize $SrO\text{-}ZnO/Al_2O_3$ heterogeneous catalyst for biodiesel production from WCO, the maximum biodiesel yield of 95.7% was obtained [18]. Ganesan et al. synthesized ammonium ferric sulfate-calcium silicate (AFS-CS) heterogeneous catalyst for free fatty acid (FFA) esterification and achieved the maximum methyl ester yield of 100% [19].

†To whom correspondence should be addressed.
E-mail: naeeem64@yahoo.com, shahzamannce@gmail.com, farooq_khann@yahoo.com

In this sense, the utilization of raw and natural resources for the heterogeneous catalyst development has been of great interest among the research society so as to address the issue of biodiesel high cost [20]. Among various natural resources, clays such as kaolin, chrysotile, bentonite, zeolite and dolomite, have been applied as an efficient heterogeneous catalyst/support after functionalization with acid, base and metal oxide for sustainable biodiesel production. Among them bentonite is extensively available and can be used as hopeful support for biodiesel technology development. Furthermore, bentonite is preferred due to its low cost, high stability, reusability, and being environmentally benign and has been studied in different research areas such as fertilizers, effluent treatment, palletizing application, adsorption and seed coating [21]. Chemically, bentonite is composed of Al, K, Ca, Si, and Na. Soetaredjo et al. synthesized KOH/bentonite catalyst for palm oil biodiesel production [22], Boz et al. fabricated KF-functionalized calcium bentonite for biodiesel production [21] and Ali et al. synthesized NaOH/bentonite for the conversion of rubber seed oil to biodiesel [23].

Therefore, in the present study, new heterogeneous bentonite based catalyst was fabricated by the impregnation of indigenous bentonite clay with ammonium persulfate (APS) to develop acid active sites (sulfate ions) on the surface of the designed catalyst to perform esterification and trans-esterification reaction simultaneously. The active sites' density of the synthesized catalyst was determined by titration method and was found to be 3.0 mmol/g. Furthermore, the designed catalyst was analyzed with various analytical tools to investigate its various physicochemical properties. Moreover, different reaction dependent variables such as oil/methanol molar ratio, reaction temperature, catalyst amount, reaction time, and stirring speed were scrutinized to investigate a suitable set of reaction parameters for maximum biodiesel production.

EXPERIMENTAL

1. Chemicals and Materials

Sufuric acid (H_2SO_4), acetic acid (CH_3COOH), potassium hydroxide (KOH), potassium iodide (KI), starch, toluene, sodium thiosulphate ($Na_2S_2O_3$), and chloroform ($CHCl_3$), were collected from Sharlau Chemical Company. Methanol, n-hexane, diethyl ether and silicon oil were supplied by Dae-Jung Chemicals and Metals company, Korea. All the chemicals used in this research work were of analytical grade.

2. Physiochemical Properties of the Selected Feedstock

The WCO was collected from the various cafeterias located under the premises of University of Peshawar. The collected WCO was filtered and then washed with hot distilled water (DW) in order to eliminate the suspended impurities. Later on, the oil was placed at 100 °C for overnight in an oven. The physicochemical characteristics of the purified WCO were determined by means of the European Standard EN 14104 and ASTM 6751 methods, whereas the fatty acid composition was determined by GC-MS as presented in the Table 1.

3. Catalyst Preparation

The APS impregnated bentonite catalyst was prepared in an aqueous medium by impregnation method. In a typical procedure, the bare bentonite clay was first crushed to very fine powder and then heated at 120 °C for overnight to escape the absorbed water molecules and other organic contaminants. The dried clay powder was then impregnated with aqueous ammonium persulfate $(NH_4)_2S_2O_8$ solution under continuous stirring and heated gently to evaporate the water molecule. Finally, the resultant slurry was collected, dried at 120 °C for overnight and kept for further instrumental and experimental analysis.

4. Acid Density Determination

Acidity index of the APS impregnated bentonite catalyst was examined by titration method. Briefly, 0.2 g catalyst was subjected into 40 ml NaCl (2 M) solution and stirred vigorously for 24 hr. The mixture was filtered to remove the catalyst and 20 ml of the titrant was titrated with NaOH standard solution (0.01 M) using few drops of phenolphthalein indicator. The volume of NaOH used was noticed for color change to pink. The total acidity index (mmol/g) of the APS impregnated bentonite catalyst was calculated using Eq. (1).

Table 1. Physiochemical propeties and chemical composition of waste cooking oil

Property	Value	Unit	Method
Acid value	20	mgKOH/g	EN1404
Saponification value	190	mgKOH/g	AOCScd 3A-94
Average molecular mass	932	g/mol	GB 5530-85
Kinematic viscosity	42	cSt	ASTMD-445
Fatty acid composition (wt%)			
Oleic acid ($C_{18}H_{34}O_2$)	28		
Tetracosanoic acid ($C_{24}H_{48}O_2$)	0.44		
Myristic acid ($C_{14}H_{28}O_2$)	12		
11-Eicosenoic acid ($C_{20}H_{38}O_2$)	1.55		
Palmitoleic acid ($C_{16}H_{30}O_2$)	33		
Linoleic acid ($C_{18}H_{32}O_2$)	15		
Eicosenoic acid ($C_{24}H_{48}O_2$)	2.1		
Other free fatty acid	1.6		
Diglyceride	1.5		
Monoglyceride	2.6		

$$\text{Acid density (mmol/g)} = \frac{V_{NaOH} \times C_{NaOH} \times V_S / V_A}{m} \quad (1)$$

V_{NaOH} is volume of NaOH used, C_{NaOH} is the concentration of NaOH, V_S is the volume of NaCl solution in which catalyst is dispersed, V_A is the volume of titrant titrated with NaOH solution and m is weight of the catalyst.

5. Catalyst Characterization

The designed APS impregnated bentonite catalyst was analyzed by different instrumental techniques to understand the various physicochemical properties. Scanning electron microscope (SEM, JSM-6490, JEOL) analysis was executed to examine the morphology and external structure of the designed catalyst. X-ray diffractometry (XRD, JDX-3532, JEOL, Japan) with the scan range of theta from 2° to 70° at a scanning rate of 5-degree per minute analysis was conducted for phase identification. While, the elemental composition (%) of the designed catalyst was identified by using energy dispersive X-rays (EDX) analysis (NCA-200) Oxford UK. Fourier transform infrared (FT-IR, Shimadzu, IR prestige -21, FT-IR-8400) spectrometry was used for qualitative and confirmative study of the functional groups present on the surface of catalyst after ammonium persulfate (APS) impregnation. To study the thermal durability of the synthesized catalyst, thermogravimetric analysis (TGA) outfitted with differential thermo-gravimetry (DTG, Diamond TG/TDA) Perkin Elmer was carried out.

6. Catalytic Performance of APS Impregnated Bentonite

The trans-esterification reaction was executed in three necked flask reactor externally connected with bulb condenser and internally connected with thermocouple for the WCO conversion to biodiesel using the synthesized catalyst. The synthesized catalyst was first dispersed in a certain amount of methanol and the mixture was stirred to activate the catalyst. Later, a known amount of WCO oil was added to the mixture and the reaction continued by changing the various reaction influencing parameters (temperature, methanol : oil molar ratio, catalyst dosage, reaction time, and stirring rate) in order to investigate a suitable set of reaction parameters for maximum biodiesel production. At the end of the reaction, solid catalyst was collected by centrifugation from reaction product and mixture of glycerol and biodiesel was shifted to separating funnel. After washing and drying the resultant biodiesel was analyzed by using GC-MS to calculate the biodiesel yield, fatty acid methyl ester (FAME) contents, and FAME conversion using the following Eqs. (1), (2), and (3).

$$\text{Biodiesel yield} = \frac{\text{Mass of the biodiesel}}{\text{Mass of the oil}} \times 100 \quad (1)$$

$$\text{FAME contents (\%)} = \frac{\Sigma A - A_S}{A_S} \times \frac{C_S \times V_S}{m} \times 100\% \quad (2)$$

$$\text{Conversion to FAME (\%)} = \frac{\Sigma A - A_S}{A_S} \times \frac{\text{Mass of the biodiesel}}{\text{Mass of the oil}} \times 100\% \quad (3)$$

ΣA=represents total peak areas of methyl ester present in the mixture
A_S=represents the peak area of internal standard (methyl octanoate)
C_S=represents the concentration (mg/ml) of methyl octanoate solution
m=mass of the sample

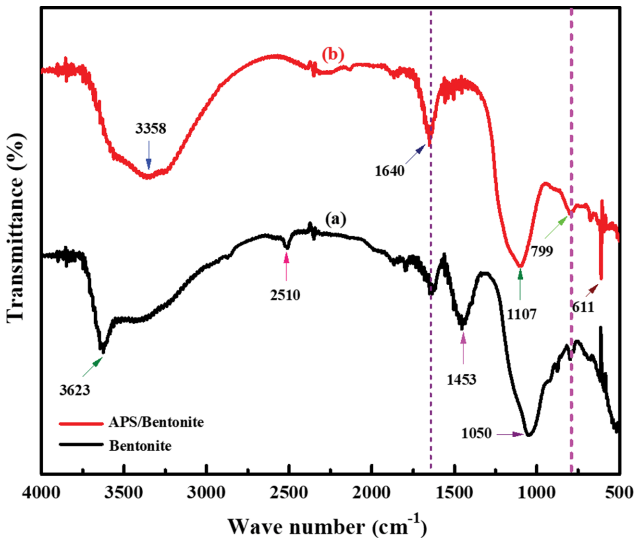

Fig. 1. FT-IR spectra of bare bentonite (a) and APS impregnated bentonite (b).

V_S=represents the volume of methyl octanoate solution used.

RESULTS AND DISCUSSION

1. Catalyst Characterization

1-1. FT-IR Analysis

The IR spectra of bare bentonite and APS impregnated bentonite catalyst are presented in Fig. 1(a), (b). The IR spectrum of bare bentonite (Fig. 1(a)) consists of various peaks ranging from 4,000 cm^{-1} to 500 cm^{-1}. The peaks at 799 cm^{-1} and 1,050 cm^{-1} are credited to the stretching mode of Si-O-Si and -S=O bond, respectively [24,25]. The peak at 1,453 cm^{-1} is assigned to C=N vibration. Similarly, the band at 1,640 cm^{-1} shows the H-OH bending vibration and the one at 2,510 cm^{-1} may be assigned to the stretching mode of CO_3^{2-}. The peak at 3,623 cm^{-1} is assigned to the stretching vibration of the strong lattice OH group [26-29]. Moreover, the IR spectrum of ammonium persulfate (APS) impregnated bentonite catalyst is shown in Fig. 1(b). The appearance of new peaks after impregnation at 611 cm^{-1} and 1,107 cm^{-1} is attributed to -SO- bending vibration, whereas the peak at 1,050 cm^{-1} is shifted to 1,107 cm^{-1} upon APS impregnation followed by calcinations at high temperature corresponding to asymmetric stretching of O=S=O bond, justifying the successful impregnation of APS over bentonite support [30,31]. Similarly, the peak at 3,358 cm^{-1} could be assigned to the stretching vibration of N-H bond [27].

Furthermore, the results obtained from EDX analysis also augment the conclusion derived from the IR spectra, where a significant increase in the sulfur content is observed after impregnation of bentonite with ammonium persulfate (APS).

1-2. Thermo Gravimetric Analysis (TGA/DTA)

A TGA–DTA analysis was carried out to determine the thermal stability of the APS impregnated bentonite catalyst. The TGA-DTA result of the designed catalyst presents three endothermic peaks as shown in Fig. 2. The peak that developed at 49 to 129 °C could be assigned to the evaporation of adsorbed water molecule (dehydra-

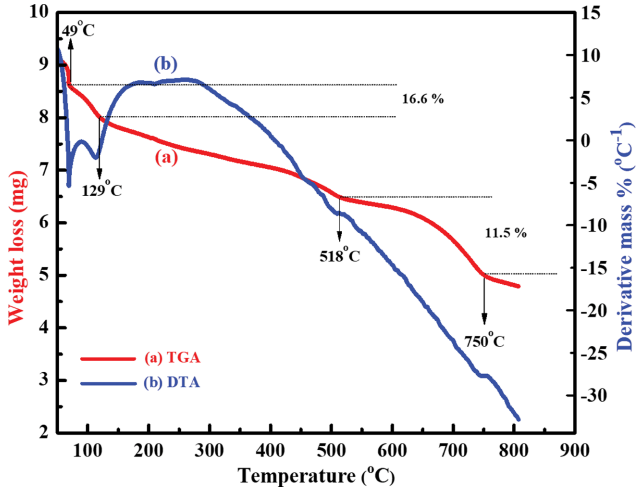

Fig. 2. TGA/DTA curves of APS impregnated bentonite catalyst.

tion) with weight loss of 16.6%. The second peak between 518 °C to 750 °C with weight loss of 11.5% corresponds to sulfate or peroxydisulfate group decomposition and SO_X emission [32]. The sulfated species is thermally stable below 518 °C and superior as compared to other reported sulfated metal oxides, which demonstrates its suitability for the catalytic trans-esterification that is performed at 75 °C [33]. However, heating beyond 750 °C results in collapsing the interlayer spaces, and consequently rupturing the bentonite structure, as reported by many researchers [34,35].

1-3. Morphological and Surface Analysis of Bare and APS Impregnated Bentonite Catalyst

The morphological properties of the synthesized catalyst and support material (bare bentonite) have been observed from SEM images as shown in Fig. 3. The surface morphology of bare bentonite (Fig. 3(a)) was granular like. However, after APS impregnation, the morphology of the bare bentonite was completely changed, showing that the APS was significantly dispersed onto the bare bentonite form, a flake like structure, as supported by XRD analysis [36]. Moreover, the EDX analysis illustrates the chemical composition of the synthesized catalyst as presented in the Table 2. It was observed that the sulfur content is significantly increased in the modified bentonite, demonstrating the existence of sulfate group on the surface of APS impregnated bentonite catalyst. The EDX result is in agreement with the reported data [37,38]. Furthermore the BET surface area and pore volume of APS impregnated bentonite (Fig. 4(a), (b)) was found to be 93 m^2/g and 0.24 cm^3/g, respectively. The decrease in surface area and pore volume could be due to the significant incorporation of APS into the pore of bare bentonite (167 m^2/g and 0.30 cm^3/g) [22].

1-4. XRD Analysis

The phase identification of the APS impregnated bentonite and bare bentonite was examined with XRD analysis as depicted in Fig. 5. The XRD analysis of bare bentonite (Fig. 4(a)) shows various reflections. The diffraction peak at 10° illustrates the tetragonal crystal of CaO, while the peak at 19.7° illustrates the triclinic silica SiO_2. The peak at 26.7° is attributed to SiO_2 (quartz) and iron aluminum silicate (Fe_3AlSiO_3) in the triclinic phase. The peaks at

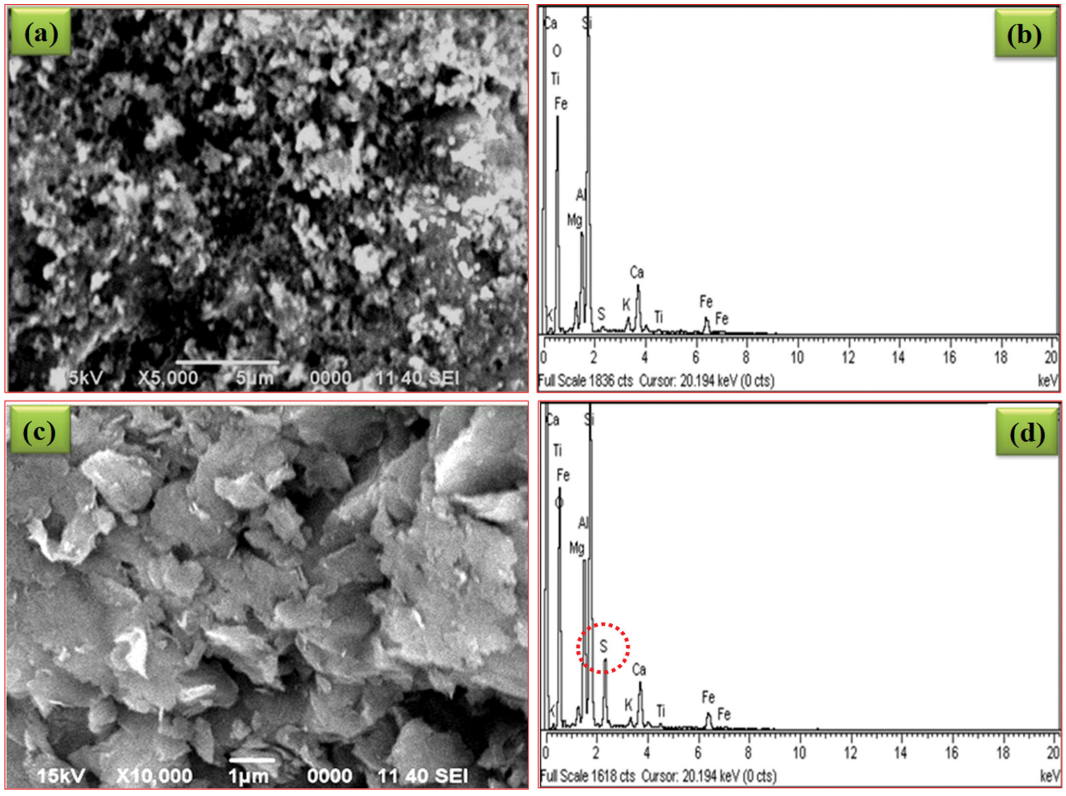

Fig. 3. SEM and EDX images of bare bentonite (a), (b) and APS impregnated bentonite (c), (d).

Table 2. Chemical composition of the APS impregnated catalyst

Catalysts	Bare bentonite		APS impregnated bentonite	
Element	Weight (%)	Atomic (%)	Weight (%)	Atomic (%)
K (Potassium)	1.19	0.62	0.68	0.36
O (Oxygen)	57.37	70.43	53.04	68.22
Ca (Calcium)	5.47	2.78	4.18	2.15
Mg (Magnesium)	2.28	1.19	1.03	0.87
Ti (Titanium)	0.36	0.15	0.30	0.13
Al (Aluminum)	6.76	5.10	9.02	6.88
Fe (Iron)	4.60	1.86	3.93	1.45
Si (Silicon)	23.57	17.08	23.02	16.87
S (Sulphur)	0.40	0.26	4.79	3.08

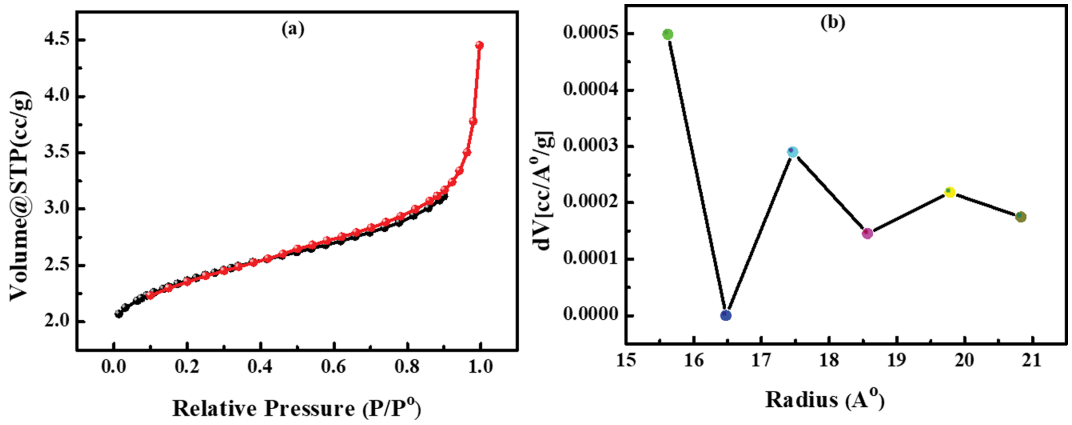

Fig. 4. (a) N_2 adsorption-desorption isotherms (b) pore size distribution of APS impregnated bentonite.

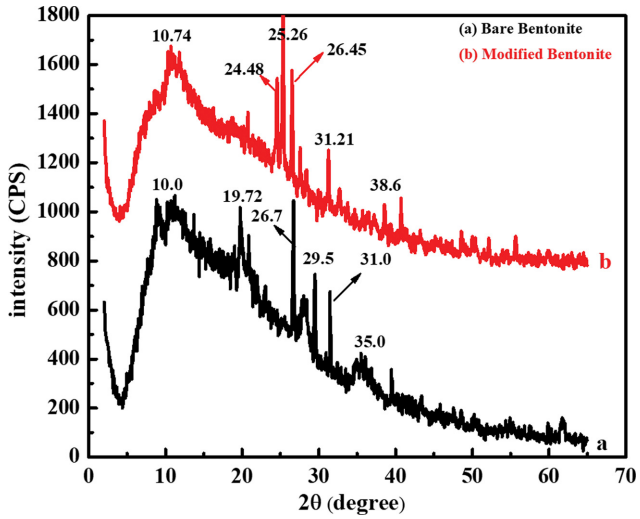

Fig. 5. The XRD patterns for bare bentonite and APS impregnated bentonite.

29.5°, 31° and 35° are attributed to cesium oxide, hexagonal CaO and hydrated silica ($SiO_2 \cdot H_2O$), respectively. On the other hand, the XRD pattern of the APS impregnated bentonite catalyst (Fig. 4(b)) shows some extra high intensity peaks. The peak at 10.7° shows tetragonal MgO, while the peaks at 24.48° and 25.26° illustrate the face centered cubic crystal of K_2O. The peaks at 26.4° and 31.2° reveal the tetragonal phase of Ca_5Si_3 and monoclinic crystal of Mg_2Ca forming oxide in combination with other oxides, respectively. While, the peak at 2-theta equal to 38.6° is attributed to the crystalline nature of K_2O [39]. Interestingly, no characteristic peak was observed for sulfate group in the XRD pattern of modified clay. This may be due to the fact that all the oxygen atoms of the sulfate group were transformed into different types of metal oxides and silicon oxides after thermal treatment (calcination). The bands shifted in diffractograms were mainly due to dehydration, which increases the inter layer distance. Moreover, the entrance of different types of metal oxides and silicon oxides causes the bands shifting, leading to increase in the surface area and enter layer distance. This investigation shows that the clay majorly consisted of more active groups of mixed oxides like SiO_2, CaO, and K_2O after impregnation with APS, which are the characteristic components of montmorillonite and kaolin clay as supported by the EDX and FTIR analysis. Therefore, at elevated temperature phase transition, variation in structure and crystal plane was recorded [40].

2. Effect of Various Reaction Parameters on Biodiesel Production

2-1. Effect of WCO : Methanol Molar Ratio

The dependence of the oil/methanol molar ratio has a significant role in biodiesel productivity. In this regard, various experiments were performed to investigate the influence of WCO : methanol

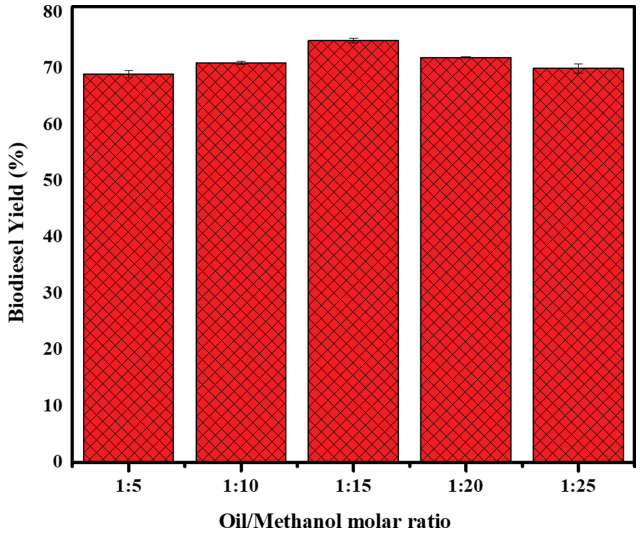

Fig. 6. Influence of methanol to oil molar ratio on biodiesel production from WCO under the reaction conditions: 2.5 wt% of catalyst amount, in 3.5 hr of reaction time at 75 °C, under the stirring rate of 600 rpm.

molar ratio on the trans-esterification reaction as given in Fig. 6. It was experienced that the FAME yield was improved as WCO : methanol molar ratio was increased up to 1 : 15. This suggests that mass transfer diffusion is enhanced as the methanol ratio is increased, which facilitates the biodiesel reaction on the product side. However, it was noticed that when the methanol ratio was further increased beyond 1 : 15 molar ratio, a significant decrease in the biodiesel yield was noted at 1 : 20 and 1 : 25 molar ratio (72% and 70%), respectively. This may be due to the solubility of glycerol in excess volume of methanol, which favors the backward reaction and decreases the overall yield of biodiesel [41-43]. The methanol hydroxyl (OH) group emulsifies the methyl ester and encourages gel formation, which makes complex purification and separation of product [44].

Table 3. Acid density of the bare and APS impregnated bentonite catalyst

Catalyst	Acidic density (mmol/g)
Bare bentonite	0.04 mmol/g
APS/bentonite	3.0 mmol/g

2-2. Effect of Catalyst Concentration

The catalytic activity of the heterogeneous catalyst depends upon the existence of active sites available on the surface of the synthesized catalyst. Different experiments were conducted by changing the catalyst concentration from 1.5-3.5 wt% (Fig. 7), while keeping constant the other reaction parameters. It can be seen that biodiesel yield was enhanced drastically with increasing the catalyst dosage in the trans-esterification reaction by providing sufficient numbers of active sites. Moreover, a decrease in biodiesel yield (68%) was observed when catalyst concentration was enhanced beyond 2.5 wt%. It could be due to the generation of viscous slurry, which influences the mass transfer rate, and therefore the biodiesel yield was decreased [45,46]. Hence, maximum biodiesel yield of 75% was achieved with 2.5 wt% catalyst concentration. This suggests that 2.5 wt% APS impregnated bentonite catalyst provides maximum number of active sites as shown in Table 3 and has been selected for the evaluation of other reaction dependent variables.

2-3. Effect of Reaction Time

The effect of reaction time is also one of the critical parameters that must be investigated to develop cost efficient biodiesel production on an industrial scale. In this regard, various trans-esterification reactions were performed at different time intervals to choose the best reaction time for maximum biodiesel production as presented in Fig. 8. The results suggest that FAME yield increases with

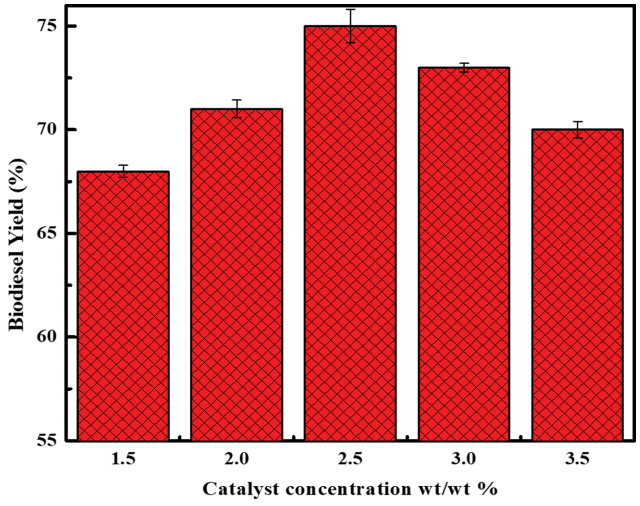

Fig. 7. Influence of catalyst concentration on biodiesel production from WCO using APS impregnated bentonite catalyst under the reaction conditions: 10 : 1 methanol to oil molar ratio, in 3.5 hr of reaction time at 75 °C, under the stirring rate of 600 rpm.

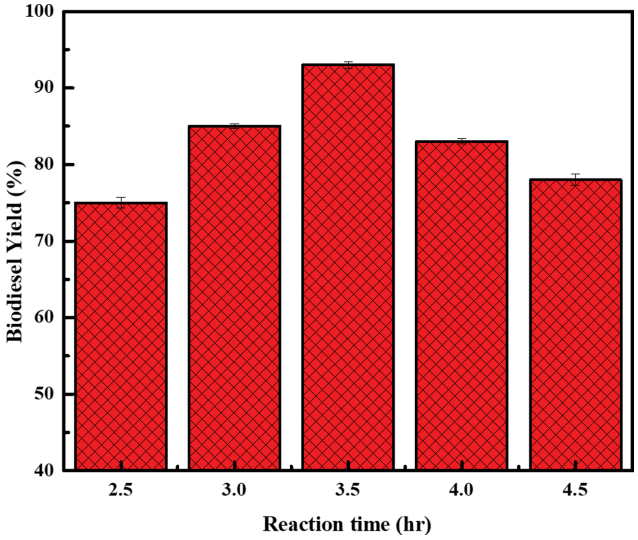

Fig. 8. Effect of reaction time on fatty acid methyl ester production from WCO using APS impregnated bentonite catalyst under the reaction conditions: 10 : 1 methanol to oil molar ratio, 2.5 wt% catalyst amount, at 75 °C, under the stirring rate of 600 rpm.

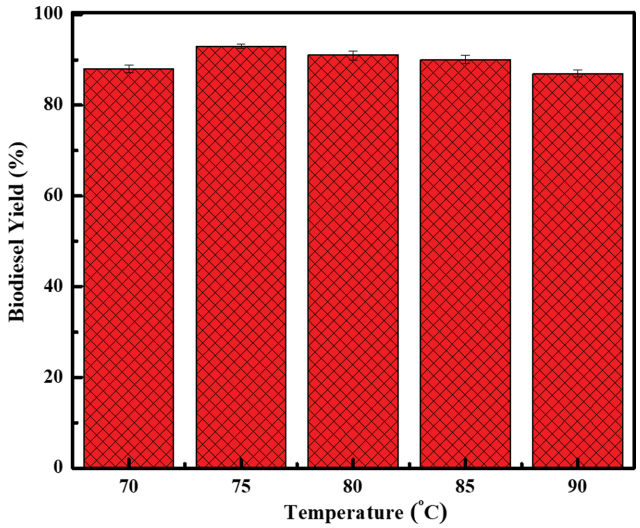

Fig. 9. Effect of reaction time on biodiesel production from WCO using APS impregnated bentonite catalyst under the reaction conditions: 10 : 1 methanol to oil molar ratio, 2.5 wt% catalyst amount, in 3.5 hr, under the stirring rate of 600 rpm.

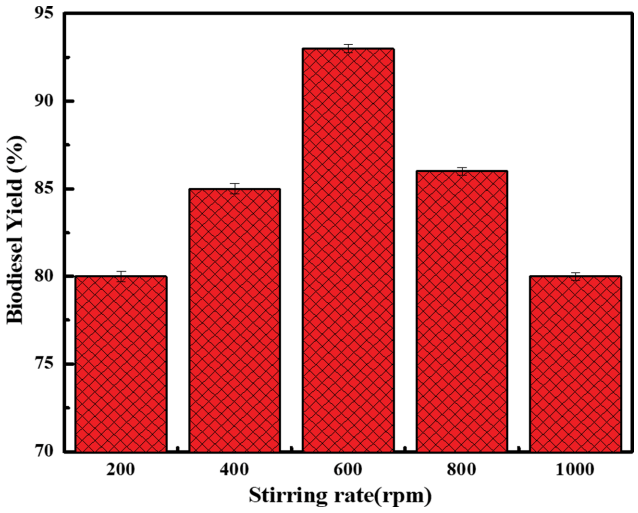

Fig. 10. Effect of stirring rate on biodiesel production from WCO using APS impregnated bentonite catalyst under the reaction conditions: 10 : 1 methanol to oil molar ratio, 2.5 wt% catalyst amount, at 75 °C in 3.5 hr of reaction time.

increasing the reaction time and optimum yield of 93% was achieved in 3.5 hr of reaction time. This could be attributed to the fact that at that a particular time reactants get enough time to interact with catalyst and converted into final product (biodiesel) as gaining equilibrium. Further, it was noticed that there was no significant increase in FAME yield when the reaction time was further prolonged. It could be due to the reversible nature of the trans-esterification reaction. Here, it is important that beyond optimum time the ester molecule has greater chance to collide with glycerol molecule and hence drives the reaction in backward direction, resulting in decline of the biodiesel yield. Therefore, a reaction time of 3.5 hr was chosen as the best reaction time for biodiesel production [47-49].

2-4. Effect of Reaction Temperature

The effect of reaction temperature on trans-esterification reaction was also evaluated for maximum biodiesel production as depicted in Fig. 9. Generally, due to the endothermic nature of the trans-esterification reaction, the FAME yield increases with increasing the reaction temperature. Herein, the reaction provided maximum biodiesel yield of 93% at reaction temperature of 75 °C, because at that particular temperature the number of fruitful collisions and K.E among the reactant molecules increases, which drives the reaction in the forward direction [50-52]. However, beyond optimal temperature (75 °C), the FAME yield was observed to decrease gradually. The decreasing trend could be due to the vaporization of methanol from reaction medium [53]. Secondly, the polarity of alcohol also decreases at a high temperature, which in turn decreases the methoxide ion formation, significantly decreasing the biodiesel yield [53,54].

2-5. Effect of Stirring Rate

Stirring speed plays an important role in overcoming the mass transfer effect, enhancing the proper contact among the reactant molecules to facilitate the forward reaction. The influence of stirring speed was examined in the range of 200-1,000 rpm during the trans-esterification reaction as presented in Fig. 10. It was recorded that the biodiesel yield was improved from 83% to 93% as the agitation speed was increased to 600 rpm. Therefore, the stirring speed of 600 rpm was selected for the efficient conversion of WCO into biodiesel by using APS impregnated bentonite heterogeneous catalyst [55,56].

2-6. Catalyst Regeneration Study

The reusability of the designed catalyst was evaluated under the best reaction conditions: WCO : MeOH molar ratio, 1 : 10; reaction temperature, 75 °C; reaction time, 3.5 hr; and catalyst concentration, 2.5 wt% for sustainable biodiesel production. The catalyst was collected, washed with n-hexane for three times after each experiment by centrifugation to reactivate it for the next run. When the catalyst was used for 1, 2, 3, 4 and 5 runs the conversion yield was obtained was 93%, 90%, 88%, 86% and 80%, respectively. The experimental results show that the solid catalyst retained its catalytic activity after the fifth run, providing the FAME yield of >80% without any significant loss in catalytic activity, demonstrating its good reusability (Fig. 11). However, beyond the fifth run the catalytic activity is decreased up to 70%. So it can be concluded that the slight decrease in the catalytic activity was mostly due to the deposition of triglycerides or other impurities (such as glycerol, ester) on the solid catalyst surface, as reported by many researchers [42,57,58]. During the course of this study and investigation, no lixiviation of the active sites from catalyst surface occurred after the trans-esterification reaction, which was confirmed by analyzing the biodiesel sample, where no active elements were detected.

To investigate the heterogeneous behavior of the designed APS impregnated bentonite catalyst, a hot filtration test was executed [59]. The WCO trans-esterification reaction was performed under the optimum reaction condition. After 60 min, the catalyst was separated from reaction mixture via filtration and the same mixture without catalyst for 160 min proceeded under the identical optimum reaction conditions. No increase was observed in the FAME

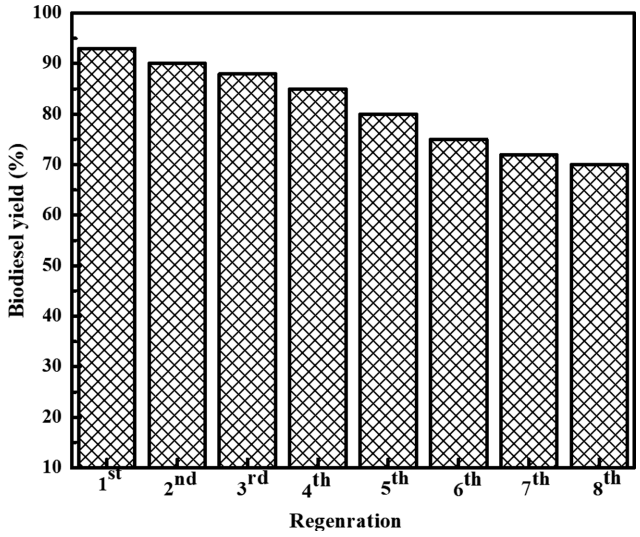

Fig. 11. Recyclability of the using APS impregnated bentonite catalyst under identical reaction conditions: 10 : 1 methanol to oil molar ratio, 2.5 wt% catalyst amount, at 75 °C in 3.5 hr of reaction time and 600 rpm.

yield, demonstrating the significant contribution and heterogeneous nature of the APS impregnated bentonite catalyst in the trans-esterification reaction [59,60].

3. GC-MS Analysis of Synthesized Biodiesel

Chemical composition of synthesized biodiesel sample was analyzed by using a gas chromatograph mass spectrometer (GC-MS). Fig. 12 presents the GC-MS chromatogram of the WCO biodiesel, and the corresponding methyl esters are given in Table 4. All the peaks appearing in the GC chromatogram were recognized by comparing with the NIST21.LIB, NIST107.LIB, WILEY229.LIB, and GC libraries.

Table 4. Ester composition of the synthesized biodiesel

Peak no	Retention time	Identified Ester from GC-MS
1	17.2	Palmitoleic acid methyl ester
2	19.5	Pentadecanoic acid methyl ester
3	21.6	Hexadecanoic acid ethyl ester
4	23.2	Octadecanoic acid, methyl ester
5	25.5	Eicosanoic acid, methyl ester
6	27.5	Docosanoioc acid, methyl ester
8	28.4	tetracosanoic acid methyl ester

Table 5. Physiochemical properties of the synthesized biodiesel

Properties	Unit	ASTM D- 6751	EN 14214	Synthesized biodiesel
Acid value	mgKOH/g	≤05	0.5	0.30
FAME content	%	>96.5	>96.5	97.3
Calorific value	J/g	_	_	41002
Viscosity	mm^2/s	1.90-6.00	3.0-5.0	3.955
Monoglycerides	% mass	_	<0.8	<0.40
diglyceride	% mass	_	<0.2	<0.07
Triglyceride	% mass	_	<0.2	<0.062
Glycerol	% mass	0.02	0.02	0.018

4. Biodiesel Characterization

The physicochemical characteristics of the WCO biodiesel were investigated by EN 14214 and ASTM-D 6751, as given in Table 5. The results suggest that the obtained biodiesel is of high quality and its physiochemical properties are comparable with the results reported by other researchers [56,61].

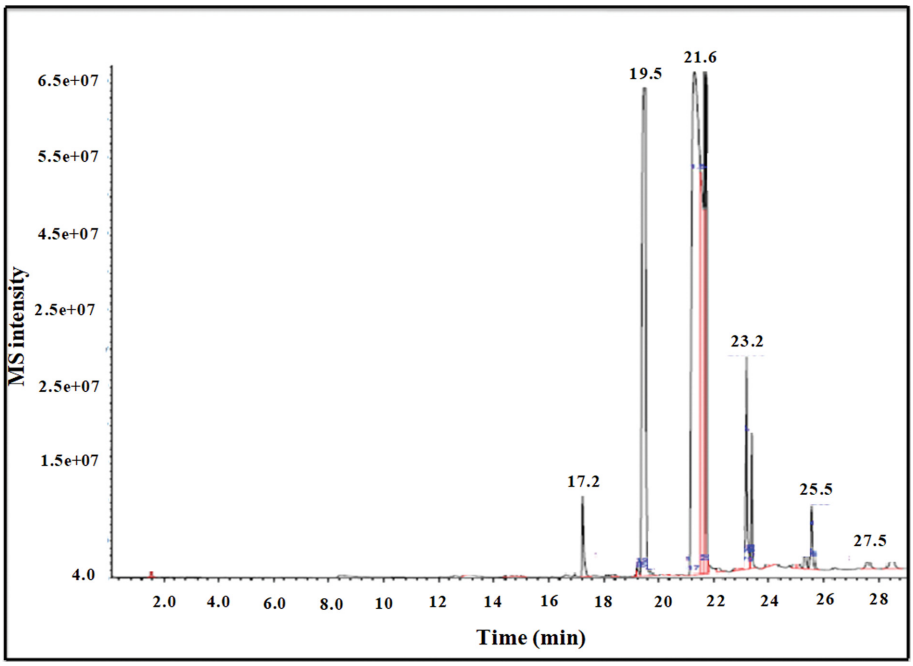

Fig. 12. GC-MS chromatogram of the synthesized biodiesel.

CONCLUSIONS

Indigenous bentonite clay was successfully modified with ammonium persulfate (APS) to develop an effective and low cost heterogeneous acid catalyst for biodiesel production. The conventional three necked flask reactor was used to evaluate the catalytic performance of the APS impregnated bentonite. The prepared catalyst showed sound catalytic activity for high acid value feedstock (WCO) conversion into biodiesel avoiding the soap formation and gave efficient biodiesel yield of 93% under the temperate reaction conditions; 10 : 1 methanol to oil molar ratio, 2.5 wt% catalyst amount, in 3.5 hr at 75 °C, under the stirring rate of 600 rpm. Moreover, it was observed that the acid impregnated bentonite has the potential to be used for up to eight cycles providing biodiesel yield of >70%. Furthermore, this study could efficiently be implemented to biovalorize the locally generated WCO for greener and sustainable energy production in the near future.

REFERENCES

1. F. Arcigni, R. Friso, M. Collu and M. Venturini, *Renew. Sustain. Energ. Rev.*, **101**, 614 (2019).
2. C. Sronsri, W. Sittipol and K. U-yen, *Chem. Eng. Sci.*, **226**, 115884 (2020).
3. D. Costa do Nascimento, N. D. Dorighello Carareto, A. Marinho Barbosa Neto, V. Gerbaud and M. C. da Costa, *Fuel*, **281**, 118717 (2020).
4. Z. Ullah, A. S. Khan, N. Muhammad, R. Ullah, A. S. Alqahtani, S. N. Shah, O. B. Ghanem, M. A. Bustam and Z. Man, *J. Mol. Liq.*, **266**, 673 (2018).
5. B. H. Jume, M. A. Gabris, H. Rashidi Nodeh, S. Rezania and J. Cho, *Renew. Energy*, **162**, 2182 (2020).
6. M. A. Amani, M. S. Davoudi, K. Tahvildari, S. M. Nabavi and M. S. Davoudi, *Ind. Crop. Prod.*, **43**, 40 (2013).
7. A. Wang, H. Li, H. Pan, H. Zhang, F. Xu, Z. Yu and S. Yang, *Fuel Proces. Technol.*, **181**, 259 (2018).
8. D. Y. Leung, X. Wu and M. Leung, *Appl. Energy*, **87**, 1083 (2010).
9. W. Ahmed, M. F. Nazar, S. D. Ali, U. A. Rana and S. U.-D. Khan, *J. Energy Chem.*, **24**, 331 (2015).
10. M. J. Borah, A. Devi, R. Borah and D. Deka, *Renew. Energy*, **133**, 512 (2019).
11. Y. A. Elsheikh, F. Elfghi, Q. Nasir and N. Muhammad, *Process Saf. Environ. Prot.*, **140**, 273 (2020).
12. M. B. Navas, I. D. Lick, P. A. Bolla, M. L. Casella and J. F. Ruggera, *Chem. Eng. Sci.*, **187**, 444 (2018).
13. B. Nath, P. Kalita, B. Das and S. Basumatary, *Renew. Energy*, **151**, 295 (2020).
14. Y. Ning and S. Niu, *Energy Convers. Manag.*, **153**, 446 (2017).
15. Q. Shu, J. Gao, Z. Nawaz, Y. Liao, D. Wang and J. Wang, *Appl. Energy*, **87**, 2589 (2010).
16. M. Hapońska, C. Nurra, S. Abelló, M. Makkee, J. Salvadó and C. Torras, *Fuel Process. Technol.*, **185**, 1 (2019).
17. M. Arrais Gonçalves, E. Karine Lourenço Mares, J. Roberto Zamian, G. Narciso da Rocha Filho and L. Rafael Vieira da Conceição, *Fuel*, **304**, 121463 (2021).
18. A. Al-Saadi, B. Mathan and Y. He, *Chem. Eng. Res. Des.*, **162**, 238 (2020).
19. S. Ganesan, S. Nadarajah, X. Y. Chee, M. Khairuddean and G. B. Teh, *Renew. Energy*, **153**, 1406 (2020).
20. A. M. Rabie, M. Shaban, M. R. Abukhadra, R. Hosny, S. A. Ahmed and N. A. Negm, *J. Mol. Liq.*, **279**, 224 (2019).
21. N. Boz, N. Degirmenbasi and D. M. Kalyon, *Appl. Catal. B: Environ.*, **138-139**, 236 (2013).
22. F. E. Soetaredjo, A. Ayucitra, S. Ismadji and A. L. Maukar, *Appl. Clay Sci.*, **53**, 341 (2011).
23. B. Ali, S. Yusup, A. T. Quitain, R. N. M. Kamil, Y. Sumigawa, M. Ammar and T. Kida, *Procedia Engin.*, **148**, 501 (2016).
24. L. Li, X. Chen, X. Xiong, X. Wu, Z. Xie and Z. Liu, *Ceram. Int.*, **46**, 19452 (2020).
25. Y. Lou, H. Cai, X. Liu, S. Tu, K. Pei, Y. Zhao, G. Cao, S. Li, K. Qin and B. Cai, *Pharmacogn Mag.*, **10**, S30 (2014).
26. K. Shimin, J. Chang and F. Juan, *Chin. J. Chem. Eng.*, **22**, 392 (2014).
27. C. Wang, Y. Hu, Q. Chen, C. Lv and S. Jia, *Biomass Bioenergy*, **56**, 405 (2013).
28. B. Hameed, C. Goh and L. Chin, *Fuel Process. Technol.*, **90**, 1532 (2009).
29. H. Zhao, C. H. Zhou, L. M. Wu, J. Y. Lou, N. Li, H. M. Yang, D. S. Tong and W. H. Yu, *Appl. Clay Sci.*, **74**, 154 (2013).
30. S. Belkharchach, H. Ighachane, A. Lachgar, M. Ait Ali and H. B. Lazrek, *J. Chem. Sci.*, **132**, 78 (2020).
31. F. Liu, X. Ma, H. Li, Y. Wang, P. Cui, M. Guo, H. Yaxin, W. Lu, S. Zhou and M. Yu, *Fuel*, **266**, 117149 (2020).
32. J. Gardy, E. Nourafkan, A. Osatiashtiani, A. F. Lee, K. Wilson, A. Hassanpour and X. Lai, *Appl. Catal. B: Environ.*, **259**, 118093 (2019).
33. S. Sen, V. Govindarajan, C. J. Pelliccione, J. Wang, D. J. Miller and E. V. Timofeeva, *ACS Appl. Mater. Interfaces*, **7**, 20538 (2015).
34. M. Toor, B. Jin, S. Dai and V. Vimonses, *J. Ind. Eng. Chem.*, **21**, 653 (2015).
35. B. Ali, S. Yusup, A. T. Quitain, M. S. Alnarabiji, R. N. M. Kamil and T. Kida, *Energy Convers. Manage.*, **171**, 1801 (2018).
36. M. J. Rezende and A. C. Pinto, *Renew. Energy*, **92**, 171 (2016).
37. M. Masteri-Farahani, M.-S. Hosseini and N. Forouzeshfar, *Renew. Energy*, **151**, 1092 (2020).
38. J. Gardy, A. Osatiashtiani, O. Céspedes, A. Hassanpour, X. Lai, A. F. Lee, K. Wilson and M. Rehan, *Appl. Catal. B: Environ.*, **234**, 268 (2018).
39. M. Feyzi and L. Norouzi, *Renew. Energy*, **94**, 579 (2016).
40. H. Alves, A. da Rocha, M. Monteiro, C. Moretti, M. Cabrelon, C. Schwengber and M. Milinsk, *Appl. Clay Sci.*, **91**, 98 (2014).
41. M. Farooq, A. Ramli and A. Naeem, *Renew. Energy*, **76**, 362 (2015).
42. I. W. Khan, A. Naeem, M. Farooq, T. Mahmood, B. Ahmad, M. Hamayun, Z. Ahmad and T. Saeed, *Renew. Energy*, **155**, 181 (2020).
43. R. F. Abdullah, U. Rashid, M. L. Ibrahim, B. Hazmi, F. A. Alharthi and I. A. Nehdi, *Renew. Sust. Energ. Reviews*, **137**, 110638 (2021).
44. M. M. Ali, R. Yunus, C. Cheng and J. Gimbun, RSC *Adv.*, **5**, 76743 (2015).
45. J. L. Aleman-Ramirez, J. Moreira, S. Torres-Arellano, A. Longoria, P. U. Okoye and P. J. Sebastian, *Fuel*, **284**, 118983 (2021).
46. A. Naeem, I. Wali Khan, M. Farooq, T. Mahmood, I. Ud Din, Z. Ali Ghazi and T. Saeed, *Bioresour. Technol.*, **328**, 124831 (2021).
47. A. R. Gupta, S. V. Yadav and V. K. Rathod, *Fuel*, **158**, 800 (2015).
48. F. Yan, Z. Yuan, P. Lu, W. Luo, L. Yang and L. Deng, *Renew. Energy*,

36, 2026 (2011).
49. K. Thinnakorn and J. Tscheikuna, *Appl. Catal. A: Gen.*, **476**, 26 (2014).
50. A. Buasri, N. Chaiyut, V. Loryuenyong, C. Rodklum, T. Chaikwan and N. Kumphan, *Appl. Sci.*, **2**, 641 (2012).
51. I. W. Khan, A. Naeem, M. Farooq, I. U. din, Z. A. Ghazi and T. Saeed, *Energy Convers. Manage.*, **231**, 113854 (2021).
52. N. J. Abd Rahman, A. Ramli, K. Jumbri and Y. Uemura, *Waste and Biomass Valorization*, **11**, 553 (2020).
53. J.-Z. Liu, Q. Cui, Y.-F. Kang, Y. Meng, M.-Z. Gao, T. Efferth and Y.-J. Fu, *Renew. Energy*, **133**, 261 (2019).
54. V. B. Veljković, O. S. Stamenković, Z. B. Todorović, M. L. Lazić and D. U. Skala, *Fuel*, **88**, 1554 (2009).
55. T. H. Dang, B.-H. Chen and D.-J. Lee, *Bioresour. Technol.*, **145**, 175 (2013).
56. M. Farooq, A. Ramli and D. Subbarao, *J. Cleaner Prod.*, **59**, 131 (2013).
57. W. Xie and H. Wang, *Renew. Energy*, **145**, 1709 (2020).
58. G. Kafuku and M. Mbarawa, *Appl. Energ.*, **87**, 2561 (2010).
59. R. Malhotra and A. Ali, *Renew. Energy*, **133**, 606 (2019).
60. I. W. Khan, A. Naeem, M. Farooq, Z. A. Ghazi and T. Saeed, *Energy Convers. Manage.*, **231**, 113854 (2021).
61. M. Farooq, A. Ramli, A. Naeem, T. Mahmood, S. Ahmad, M. Humayun and M. G. U. Islam, *Chem. Eng. Res. Des.*, **132**, 644 (2018).